Samir Zahaf[1], Noureddine Zina[2], Sabik Bouaziz[2], Boualem Chetti[1], Mustapha Kaid[3], Abdessamad Abouda[3], Zahra Najafi Vafa[4]

OPTIMIZATION OF FSW WELDING PARAMETERS ON MAXIMAL TEMPERATURE, VON MISES AND RESIDUAL STRESSES, AND EQUIVALENT PLASTIC DEFORMATION APPLIED TO A 6061 ALUMINIUM ALLOY

OPTIMIZACIJA PARAMETARA ZAVARIVANJA TRENJEM SA MEŠANJEM, MAKSIMALNE TEMPERATURE, FON MIZES I ZAOSTALIH NAPONA I EKVIVALENTNE PLASTIČNE DEFORMACIJE KOD LEGURE ALUMINIJUMA 6061

Originalni naučni rad / Original scientific paper
UDK /UDC: 621.791.1:669.75

Rad primljen / Paper received: 6.08.2019

Adresa autora / Author's address:
[1)] Depart. of Mech. Eng., National Polytechnic School of Oran Maurice Audin, Algeria email: noureddinez71@yahoo.fr
[2)] Depart. of Science and Technology, University of Khamis Meliana, Ain Defla, Algeria
[3)] Depart. of Mechanical Engineering, University of Djillali Liabes, Sidi Bel Abbes, Algeria
[4)] Department of Agronomy and Plant Breeding, Faculty of Agriculture, University of Kurdistan Sanandaj, Iran

Keywords
- FSW process
- numerical medialization
- Von Mises stress
- plastic equivalent strain
- residual stress

Ključne reči
- postupak FSW
- numerička medijalizacija
- fon Mizes naponi
- ekvivalentna plastična deformacija
- zaostali napon

Abstract

Friction stir welding (FSW) has become an important welding technique to join materials that are difficult to weld by traditional fusion welding. The model in this study is a simplified version of the thermomechanical model developed by Zhu and Chao for FSW of aluminium alloy A6061-T6. Zhu and Chao presented nonlinear thermal and thermomechanical simulations using finite element analysis code - Ansys APDL 16.2. They initially formulated a heat transfer problem using a moving heat source, and later used the transient temperature outputs from thermal analysis to determine maximum temperature, Von Mises stress, equivalent plastic strain and residual stresses in welded plates via a 3D elastoplastic thermomechanical simulation. In the first part we fixed the rotation speed and varied the welding speed (600 rpm; 80, 100, and 140 mm/min). The objective is to study the variation of transient temperature and distribution of Von Mises stress, equivalent plastic strain and evaluate the residual stress in a friction stir welded plate of A6061-T6. Results show that the simulation peak temperature is approximately near the measured one. However, the peak temperature of welded joints increases by increasing the welding frequency rotation for the same tool profile and welding speed. Residual stresses are affected by the FSW process, moreover, processing parameters influence the types of resultant stress, welding temperature and mixing. An increase in welding speed apparently has led to an increase in the residual stress. Residual stresses found by this FE model have never exceeded 54 % of the elastic limit. We conclude that the model gives a good result in terms of stress and the obtained results give a good theoretical basis for aluminium welding by FSW.

Izvod

Zavarivanje trenjem sa mešanjem (FSW) je postao veoma značajan postupak zavarivanja materijala koji se teško spajaju tradicionalnim postupkom zavarivanja topljenjem. Dat je model koji predstavlja pojednostavljenu verziju termomehaničkog modela koji su razvili Žu i Čao za FSW zavarivanje legure aluminijuma A6061-T6. Žu i Čao su predstavili nelinearne toplotne i termomehaničke simulacije, primenom programa za analizu konačnim elementima, Ansys APDL 16.2. Prvo su formulisali problem prostiranja toplote primenom pokretnog izvora toplote, a kasnije su upotrebili rezultate prelazne temperature u toplotnoj analizi, radi određivanja maksimalne temperature, napona fon Mizesa, ekvivalentne plastične deformacije i zaostalih napona kod zavarenih ploča, primenom 3D elastoplastične termomehaničke simulacije. U prvom delu smo regulisali brzinu rotacije i varirali brzinu zavarivanja (600 min^{-1}; 80, 100 i 140 mm/min). Cilj je istraživanje promene prelazne temperature i raspodela napona fon Mizesa, ekvivalentne plastične deformacije i proračun zaostalog napona kod ploče A6061-T6 zavarene trenjem uz mešanje. Rezultati daju bliske vrednosti maksimalne izmerene temperature i dobijene simulacijom. Najveća temperatura raste sa porastom frekvencije brzine rotacije kod istog profilnog alata i brzine zavarivanja. Na zaostale napone utiče postupak FSW, a parametri postupka na rezultujuće napone, temperaturu i na mešanje. Povećanje brzine zavarivanja je dovelo do porasta zaostalih napona. Zaostali naponi dobijeni ovim MKE nisu prelazili 54 % granice elastičnosti materijala. Zaključuje se da model daje dobre rezultate s obzirom na veličinu napona, a dobijeni rezultati predstavljaju dobru teorijsku osnovu za zavarivanje aluminijuma postupkom FSW.

INTRODUCTION

Friction stir welding (FSW) is a relatively new, state of the art, solid state joining process. This metal jointing technique is derived from the conventional friction welding. In a typical FSW, a rotating cylindrical pin tool is forced to plunge into the plates to be welded (i.e. workpiece) and move along their contact line (Fig. 1). During this operation, frictional heat that is generated by contact friction between the tool and workpiece softens the material.

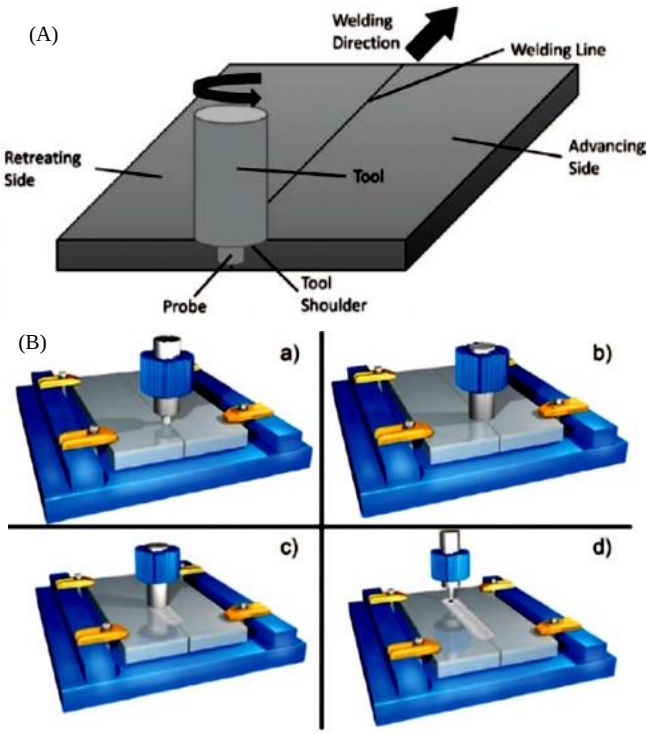

Figure 1. (A) Scheme of FSW process; (B) scheme of FSW process steps: (a) rotating tool before plunging, (b) plunging and then tool shoulder touches the work piece surface producing frictional heat, (c) rotating tool traverses along the work piece, and (d) pulling out from the workpiece.

The plasticized material is stirred by the tool and forced to 'flow' to the side and the back of the tool, as the tool advances. As the temperature cools down, a solid continuous joint between the two plates is then formed. Because the highest temperature in the FSW process is lower than the melting temperature of the workpiece material, FSW yields fine microstructures, absence of cracking, low residual distortion and no loss of alloying elements, that are the main advantages of this solid phase process. Nevertheless, as in traditional fusion welds, a softened heat affected zone and a tensile residual stress parallel to the weld also exist.

Although it is a new welding technology, the FSW has been extensively studied in both the academic and industrial communities for most aluminium alloys including difficult-to-weld alloys such as AA2195 (with lithium) and AA7075. To date, most of the researchers focused their attention on the heat transfer or temperature analysis of FSW. Atilla Savaş /1/ presented *Investigating the influence of tool shape during FSW of aluminum alloy via CFD analysis*. J. Fabregas Villegas et al. /2/ studied a *Coupled rigid-viscoplastic numerical modeling for evaluating effects of shoulder geometry on friction stir-welded aluminum alloys*. Tang et al. /3/ presented experimentally measured temperature distributions of the workpiece in an FSW. Gould and Feng /4/ proposed a simple heat transfer model for predicting the temperature distribution in the workpiece of the FSW. Chao and Qi /5, 6/ developed a moving heat source model in a finite element analysis and simulated the transient temperature, residual stress and residual distortion of the FSW process.

Furthermore, Colegrove et al. /7/ and Frigaard et al. /8/ developed three-dimensional heat flow models for the prediction of temperature fields in the FSW. Midling /9/, Russell and Sheercliff /10/ investigated the effect of tool shoulder material and pin tool on heat input during FSW. Most currently, Donne et al. /11/ reported the measured residual stresses in friction stir welds for 2024-T3 and 6013-T6 aluminium. Dong et al. /12/ carried out a coupled thermomechanical analysis of the FSW process using a simplified two-dimensional axisymmetric model. Chao et al. /13/ investigated variations of heat energy and temperature produced by FSW in both the workpiece and the pin tool. All investigations show that the FSW process of aluminium alloys yields welds with low distortion, high quality and low cost. Consequently, better structural performance is the primary advantage of this technology's applications. For example, a demonstration of the tremendous potential and successful applications of aluminium FSW in airframe structures can be found in Talwar et al. /14/.

In principle, the FSW process can be applied to joining other alloy materials such as steels and titanium as well. Of course, it is well known that current tool materials used in the FSW for aluminium are not adequate for production applications in many of the harder alloy materials. However, when adequate wear resistant tool materials become available, the benefits of FSW may promote its rapid implementation in the production of ferrous structures and structures made of other more refractory materials. While work to develop the necessary tool materials continues, it is also important to make progress in the development of the FSW process for steel.

For instance, experimental studies of austenitic stainless steels /15/ revealed the microstructures, residual stresses and strength of friction stir welds. To further understand the fundamental mechanisms associated with the welding formation process and improve the welding quality for the FSW of steel, numerical modelling and simulation of transient temperature and residual stress is valuable and needed. In this paper, a three-dimensional model based on a finite element method (FEM) is proposed to analyse the residual stress distribution in the weld, study the thermal impact and evolution of Von Mises stresses in the weld by considering the mechanical effect of the tool (only the shoulder is included at this time).

This study is accomplished by parametrically studying the effects of varying welding parameters, primarily the traverse and rotating speed of the tool. The entire welding process is simulated using the commercial finite element package ANSYS APDL 16.2. For boundary conditions we

chose rotation speed of 600 rpm and three tool feed speeds (80, 100, and 140 mm/min) so that we could compare and validate the FE model. The coordinate system adopted in our case is related to the workpiece. The purpose of this paper, a three-dimensional model based on a finite element method, is proposed to study the thermal history and Von Mises stress distribution in the weld and, subsequently, calculate the equivalent plastic strain in the longitudinal and transverse direction, and to determine the residual stresses in the weld bead.

MATERIALS AND METHODS

Geometry configuration

The welding process is shown in Fig. 2, where V is the traverse speed of the tool, and ω is the rotational speed. The tool is made of AISI A2 steel, and consists of the shoulder with diameter R_0 = 16 mm. Welded plates are 6061 Al alloy; each is of rectangular shape 200×50×3.18 mm. The tool is considered a rigid solid, and the workpiece a ductile material characterized with elasticity, plasticity, and a kinetic hardening effect. Temperature dependent properties of 6061 Al alloy are used up to 571 °C based on Ref. /8/, and are given in Table 1.

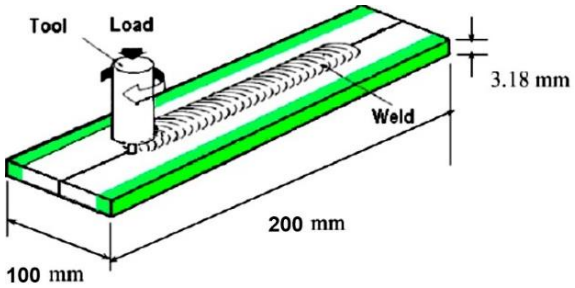

Figure 2. Geometry configuration of friction stir welding.

Table 1. Material properties of AISI A2 steel /14, 15/ and aluminium alloy 6061-T6 /16/.

	Temperature (°C)	Thermal conductivity (W/m°C)	Heat capacity (J/kg°C)	Density (kg/m^3)	Young's modulus (GPa)
AISI A2 steel		23.8	1096	7860	203
Al alloy 6061-T6	0	162	917	2703	69.7
	93.3	177	978	2685	66.2
	204.4	192	1028	2657	59.2
	315.6	207	1078	2630	47.78
	427.7	223	1133	2602	31.72
	571.1	253	1230	2574	0
	Temperature (°C)	Yield strength (MPa)	Thermal expansion (μm/°C)	Poisson's ratio	Melting Point (°C)
AISI A2 steel			10.6	0.23	
Al alloy 6061-T6	0	277.7	22.4		
	93.3	264.6	24.61		
	204.4	218.6	26.6	0.23	582-652
	315.6	66.2	27.6		
	427.7	17.9	29.6		
	571.1	0	34.2		

Inverse analysis method for heat transfer

At the present work, thermal and thermomechanical analysis is adapted, which is similar to the numerical simulation of conventional arc welding, /17, 18/. Heat transfer analysis is performed first, and the transient temperature outputs from this analysis are saved for the subsequent thermomechanical analysis. In the thermal analysis, the transient temperature field T is a function of time t and spatial coordinates (x,y,z), and is determined by the three-dimensional nonlinear heat transfer equation, /19/,

$$k\left(\frac{\partial^2 T}{\partial x^2}+\frac{\partial^2 T}{\partial y^2}+\frac{\partial^2 T}{\partial z^2}\right)+Q_{int}=c\rho\frac{\partial T}{\partial t}, \qquad (1)$$

where: k is the coefficient of thermal conductivity; Q_{int} is internal heat source rate; c is the mass-specific heat capacity; ρ is the density of material. Heat flux to the system is introduced by a moving source on the boundary of the weld line. This heat, produced by friction contact between the pin tool and the plates, is concentrated locally, and propagates rapidly into remote regions of the plates by conduction, according to Eq.(1), as well as by convection and radiation through the boundary.

It is assumed that heat flux, $q(r)$, is linearly distributed in the radial direction of the pin tool shoulder, and has the following form /4/,

$$q(r)=\frac{12Qr}{\pi\left(d_o^3-d_i^3\right)} \quad \text{for} \quad \frac{d_i}{2}\le r\ge\frac{d_o}{2}, \qquad (2)$$

where: d_o is the outside diameter of the pin tool shoulder; d_i is the pin diameter; Q is the total heat input energy. In Eq.(2), the heat generated at the pin of tool is neglected because this heat is very small, e.g. the order 2 % of total heat as reported by Russell and Sheercliff /8/. As such, in the analysis $d_i = 0$ in Eq.(2) is used.

At the boundary or surfaces of the workpiece, convection and radiation in heat transfer are responsible for heat loss to the ambient. To consider such heat convection and radiation on all plate surfaces except for the bottom surface, the heat flux loss is evaluated by

$$q_c=\beta(T-T_0)+\varepsilon B(T^4-T_0^4).$$

The chemical composition of 6061-T6 aluminium alloy is given in Table 2.

Table 2. Chemical composition AA6061-T6 /20, 21/.

Mg	Si	Fe	Cu	Zn	Ti	Mn	Cr	Al
0.8-1.2	0.4-0.8	0.7	0.15-0.40	0.25	0.15	0.15	0.04-0.35	balance

Thermomechanical model

In the thermomechanical analysis, the incremental theory of plasticity is employed. The plastic deformation of the material is assumed to obey the Von Mises yield criterion and the associated flow rule. The relationship of the rate components between thermal stresses, $\dot{\sigma}_{ij}$, and strains, $\dot{\varepsilon}_{ij}$, is described by:

$$\dot{\varepsilon}_{ij}=\frac{1+\nu}{E}\dot{\sigma}_{ij}-\frac{\nu}{E}\dot{\sigma}_{kk}\delta_{ij}+\lambda s_{ij}+\left[\alpha+\frac{\partial_\alpha}{\partial T}(T-T_0)\right]\dot{T}, \qquad (3)$$

where: E is Young's modulus; ν is Poisson's ratio; α is the thermal expansion coefficient; $s_{ij} = \dot{\sigma}_{ij} - \frac{1}{3}\dot{\sigma}_{kk}\delta_{ij}$ are components of deviatory stresses; λ is the plastic flow factor, $\lambda = 0$ for elastic deformation, or $\sigma_e < \sigma_s$, and $\lambda > 0$ for plastic deformation, or $\sigma_e \geq \sigma_s$. Here, σ_s is the yield stress; $\sigma_e = \left(\frac{3}{2}s_{ij}s_{ij}\right)^{1/2}$ is the Von Mises effective stress.

It is well known that the thermomechanical analysis for welding simulation using finite element method is extremely time consuming. To reduce computational time and still maintain reasonable accuracy, many thermomechanical numerical analyses use a 'cut-off temperature', i.e. in the mechanical properties above, the cut-off temperature is assumed to maintain constant value, /17/.

Tekriwal and Mazumder /17/ showed that residual stresses from FEA have only small changes for carbon steels when the cut-off temperature varies from 600 to 1400 °C, but the computational time is significantly reduced if cut-off temperature 600 °C is used. A cut-off temperature of 900 °C (i.e. about two-thirds of 1400 °C, melting temperature of 304L stainless steel) is used in the current numerical calculations to reduce unnecessary computational time.

Mesh, loads and boundary conditions

The mesh used in the calculations of the present study is presented in Fig. 3. It is composed of 7891 elements. The type of mesh used in this work is SOLID226 (Fig. 4), the reason for which this type of element is selected is that it has structural capabilities including elasticity, plasticity, large strain, large deflection, stress stiffening effects, pre-stress effects and structural-thermal capabilities. Figure 3 illustrates the geometry of this element /22/.

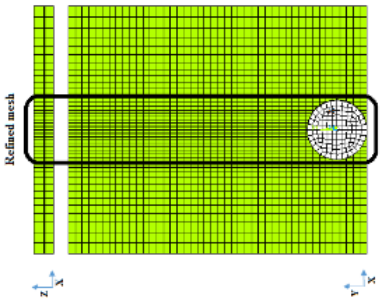

Figure 3. Finite element model meshing.

This mesh is composed of two minimum elements in the thickness in order to take into account the gradients of the thermo-mechanical quantities according to the thickness. Near the tool, a very fine mesh zone is imposed in order to take into account the boundary layer appearing in this zone.

Boundary conditions applied to the model concern both mechanical and thermal aspects. It is considered that we model welding with a given speed, v, and rotation speed of tool, ω. In the present model, the surfaces to be joined come into contact. A standard surface-to-surface contact pair using TARGE170 and CONTA174, is shown in Fig. 5.

Because of frictional contact between the tool and workpiece, responsible for heat generation, we choose a standard surface-to-surface contact pair between tool and workpiece. The CONTA174 element is used to model the contact surface on the top surface of the workpiece, and the TARGE170 element is used for the tool, as shown in Fig. 6.

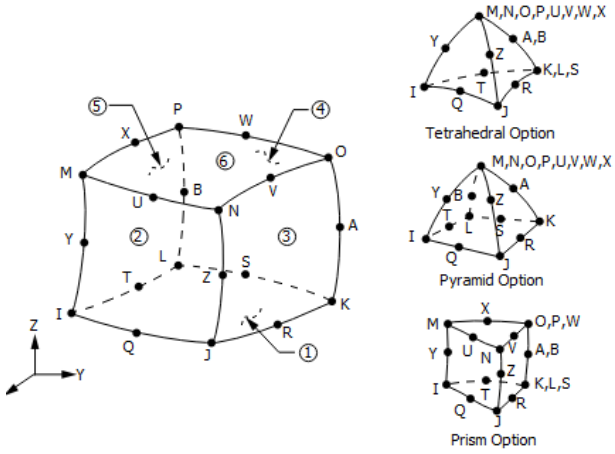

Figure 4. SOLID226 geometry.

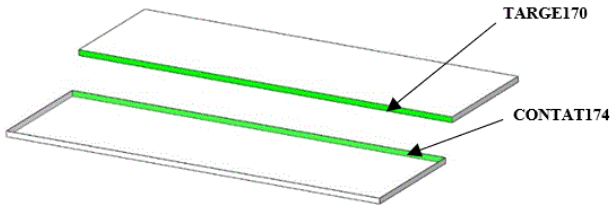

Figure 5. The contact pair between the two surfaces.

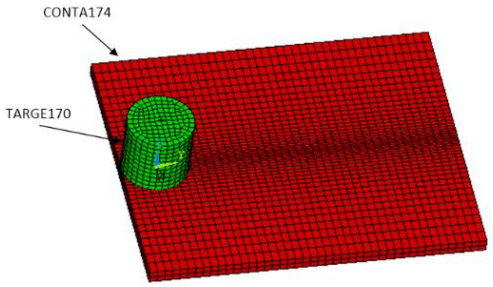

Figure. 6. The contact between the work-piece and the tool.

Thermal boundary conditions are expressed either in terms of imposed temperature, or in terms of heat. They are applied on various surfaces constituting the border:

- input: an input temperature equal to the ambient temperature, T_{amb}, is imposed;
- output: a zero heat flux, $Q = 0$, is imposed.
- lateral: a convective heat, corresponding to exchange with the unmodelled part, is applied: $Q_{lat} = h_{lat}(T - T_{amb})$.
- lower surface: convective heat corresponding to exchange with the support plate is applied: $Q_{low} = h_{low}(T - T_{amb})$.
- upper surface: convective heat corresponding to exchange with air is applied: $Q_{air} = h_{air}(T - T_{amb})$ with $h_{air} = 20\ \mathrm{Wm^{-2}K^{-1}}$ commonly accepted in literature /23/ (we do not take into account the clamping).
- pion and shoulder: a zero heat, $Q = 0$, is imposed.

Mechanical boundary conditions are expressed either in terms of imposed speed or in terms of pressure or displacement. They are applied on various surfaces constituting the border. As shown in Fig. 7, null displacements are imposed at both ends of plates and at the bottom surface of these two plates. In the first part, a fixed rotational speed is imposed

ω = 500 rpm for the tool, with board speed equal to 2 mm/s. The feed speed of the tool is also set at 140 mm/min. The preheating time is 4.5 s. These parameters are chosen to enable us to validate our numerical model with the experimental results of Chen et al. /24/.

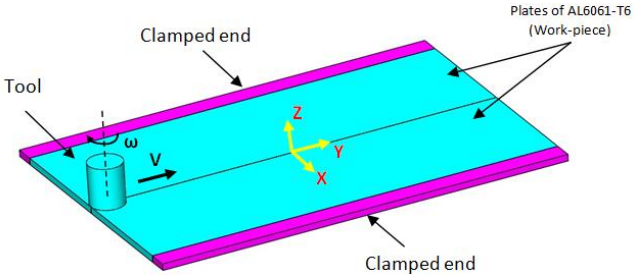

Figure 7. Configuration and boundary conditions.

Subsequently, we researched the welding parameters, such as angular and linear speed. To make a comparative study of these results. we chose angular speed of 600 rpm and welding speeds 80, 100 and 140 mm/min.

RESULTS AND DISCUSSION

Temperature distribution

Numerical investigation of heat generation in friction stir welding (FSW) of pure aluminium A6061 is performed. Simulated temperature history of FSW for pure aluminium A6061 at different process parameter combinations is shown in Fig. 8. Temperature variation with distance is shown for welding speeds 80, 100 and 140 mm/min at constant rotational speed of 600 rpm. It is evident from Fig. 8 that keeping the applied force and rotational speed constant, as welding speed increases the peak temperature decreases.

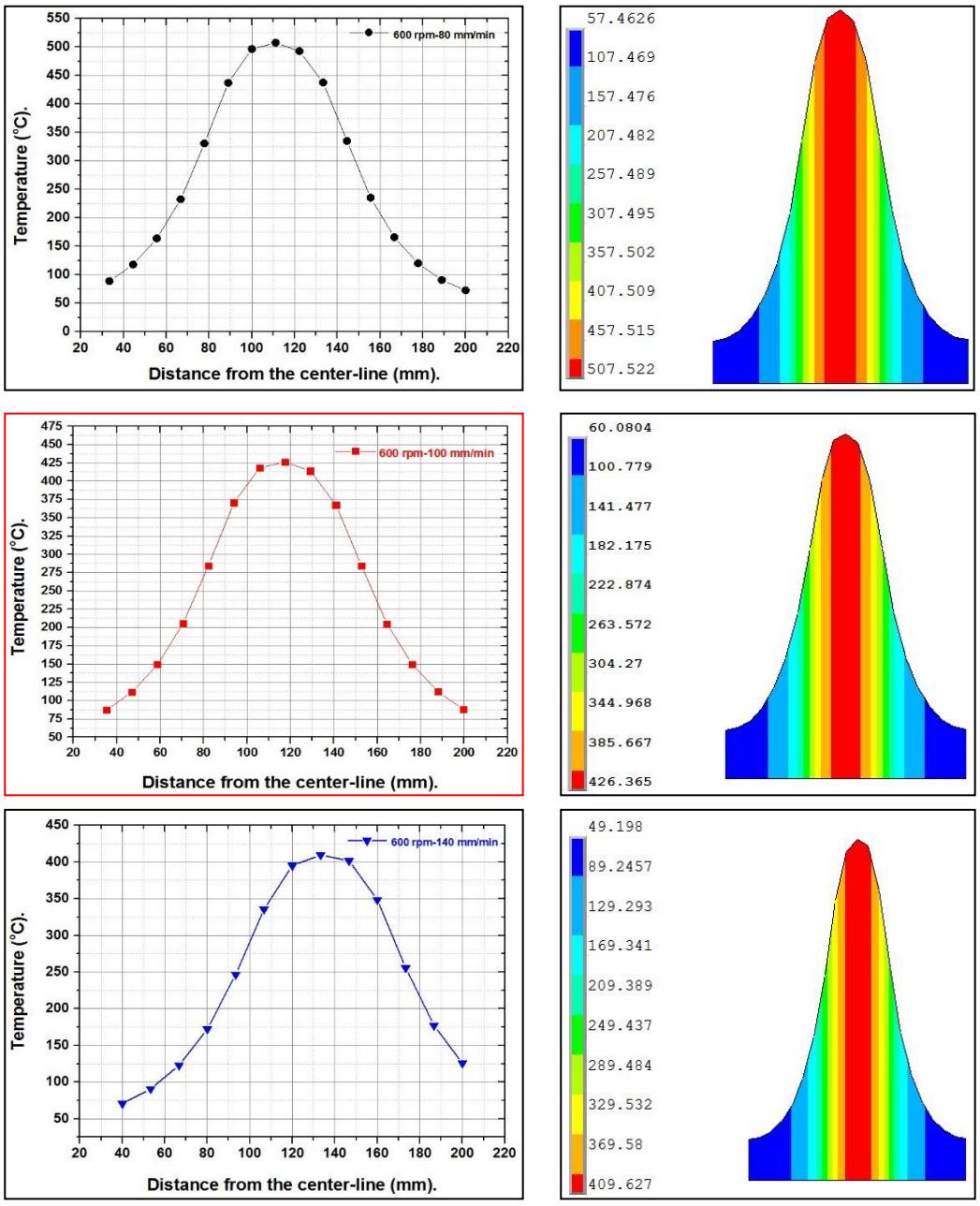

Figure 8. Temperature profiles for pure aluminium 6061 at different transverse speeds (constant rotational speed of 600 rpm).

However, at constant rotational speed of 600 rpm, it is observed that higher transverse speeds lead to lower temperatures in the stir zone and by increasing the transverse speed from 80 to 140 mm/min leads to significant variation in thermal history, where maximal temperature 507.52 °C is observed at 80 mm/min and 600 rpm.

However, to attain a good processed zone, the optimal operating temperature for material Al6061 is between 409 °C and 507 °C. As the coefficient of friction and the radius of the shoulder and pin are constant in the current investigation, the increase in welding speed needs to be compensated by decreasing the applied force. Similarly, as the welding speed increases, the contact time per unit area of tool - workpiece interface is reduced, thus reducing the peak temperature.

These observations are consistent with other studies /25/. It is clear that the softening degree of the stir zone is affected by the peak temperature and the duration of the process at high temperature. The exposed duration at three process parameters (80, 100 and 140 mm/min and 600 rpm) is 126.5, 112.5, and 96.5 s, in respect. It is clear that the cooling rate at 80 mm/min and 600 rpm, is higher than at other two transverse speeds (100 and 140 mm/min). Further, higher transverse speed will reduce the processing time and subsequently, the workpiece will be exposed to higher temperatures for a shorter time.

Analysis of the distribution of Von Mises stresses and temperature field in the welding cord

The stress will form in the weld during welding since the expansion of material occurs during the heating of the welded plates, followed by the contraction during the cooling of the welds. Furthermore, the rotational and the transverse movements of the tool will cause additional stress in the weld due to the mechanical constraint of the plates by the fixture. One of the most important features of the proposed model is the ability to predict the stress distributions (active stress and residual stress) over the whole FSW process.

Figure 9 shows Von Mises stress plots (N/m^2) at 12 characteristic times, t = 10, 20, 30, 40, 50, 60, 70, 80, 90, 100 and 112.5 s from the start of the process. At the plunging stage, an axial force is exerted on the material beneath the tool pin causing an area of high compressive stress in the workpiece. With the increasing heat at the pin-workpiece interface, the material progressively softens. We show that for a compression load P on the plate, the equivalent stresses are concentrated between the two plates and the lower surface of the tool, and are respectively equal to 1740, 1410, 1410, 1650, 2130, 2080, 2760, 3220, 242, 2140, 1430, and 1510 MPa, as depicted in Fig. 9.

In Fig. 10 at 10 s we find that the stress in the plates under the tool pin approach 1740 MPa because of extremely high temperature in this zone, equal to 587.60 °C, indicated by the equation constituent. After 10 s the maximal stress has migrated to somewhere remote from the pin-workpiece interface. However, at welding times 20, 30, 40 s, there remains a cylindrical layer of material surrounding the tool spindle with a fairly low stress at 10 s, as shown by the Von Mises stress plot. After the tool shoulder touches the workpiece at 4.5 s (preheating time), the cylindrical high stress layer gradually disappears since the material is heated by generated heat at the shoulder-pin interface. Linear welding speed at 80 mm/min with rotational tool speed 600 rpm indicate that Von Mises stress at welding times 50, 60, 70, 80, 90, and 100 s is depicted by very high contour in red (Fig. 9). Furthermore, after 100 s welding time, the Von Mises stresses are reduced and equal to 1530 MPa.

The model can predict temperature evolution through the whole process and over the whole volume. Figure 10 shows temperature distribution (°C) at twelve representative time intervals: t = 10, 20, 30, 40, 50, 60, 70, 80, 90, 100, 110 and 126.5 s. When only the pin is in contact with the workpiece, the maximal temperature in the workpiece occurs somewhere adjacent to the edge of the pin bottom surface. At 4.5 s (preheating time), the shoulder surface starts contact with the workpiece, thereafter, the maximal temperature moves towards the corner between pin and shoulder surfaces. At 10 s the full contact condition is established between tool surface and top surface of workpiece, with maximal temperature around the shoulder workpiece interface.

In Fig. 10 the simulated temperature field is shown during the steady-state welding process. It can be seen clearly that the temperature distribution is asymmetrical around the weld centreline, caused by the non-uniform material flow around the tool.

Also, we see in Fig. 10 the high temperature region located under the shoulder, where the energy density is extremely high. The peak temperature is located at the position of the advancing side behind the tool, and its value 587 °C is about 100 % of melting temperature (583 °C) of Al6061-T6 aluminium alloy. It should be noted that the temperature distribution characteristics above are similar to those in literature, /26/.

Figure 10 shows the temperature distribution in the two aluminium A6061-T6 plates treated at rotational speed of 600 rpm and transverse speed 80 mm/min at different welding times t = 10, 20, 30, 40, 50, 60, 70, 80, 90, 100 and 112.5 s. It is observed that temperatures on the advancing side are slightly higher than those in the retreating side in all combinations of process parameters. After a dwelling time, or preheating time, 4.5 and 10 s, the temperature is more evenly distributed between the front and the rear side of the tool, equal to 587.60 °C.

Then the tool began to cross to join plates. The welding process quickly reached a stable state and the distribution pattern of the temperature around the tool showed little variation, as indicated at 10 and 20 s in Fig. 10. On the other hand, in this figure we find the welding temperature decreases to 392.79 °C between 10 and 20 s. We see that the temperature contour looks almost symmetric along the joint line on both the retreating and advancing sides. This means the rotating motion of the tool will not significantly affect the temperature distribution in the workpiece.

Figure 10 shows the simulated contour of temperature change during FSW for various process parameters using ANSYS 16.2. Analysis shows that along the direction of the FSW, the temperature values increase as the time duration

increases. After a 30 s weld time, at 60 s, the temperature value has decreased to 472.18 °C but was better distributed between the front and the back side of the tool. A compression loading *P*, applied on the upper surface of the tool clearly shows the increase in temperature between the three times, 70, 80, and 90 s, equal to 486.74, 494.94, and 493.17 °C, as mentioned in Fig. 10.

Figure 10 shows the temperature distribution along a longitudinal line at the bead that is above the part to be welded to the environment of heat source. These distributions are represented at different times for aluminium alloy A6061-T6. We also observe that after the first nine instants (100, 110, and 126 s) the maximal temperature values become very close, which is due to the approximation of the source to the longitudinal sampling line (measurement).

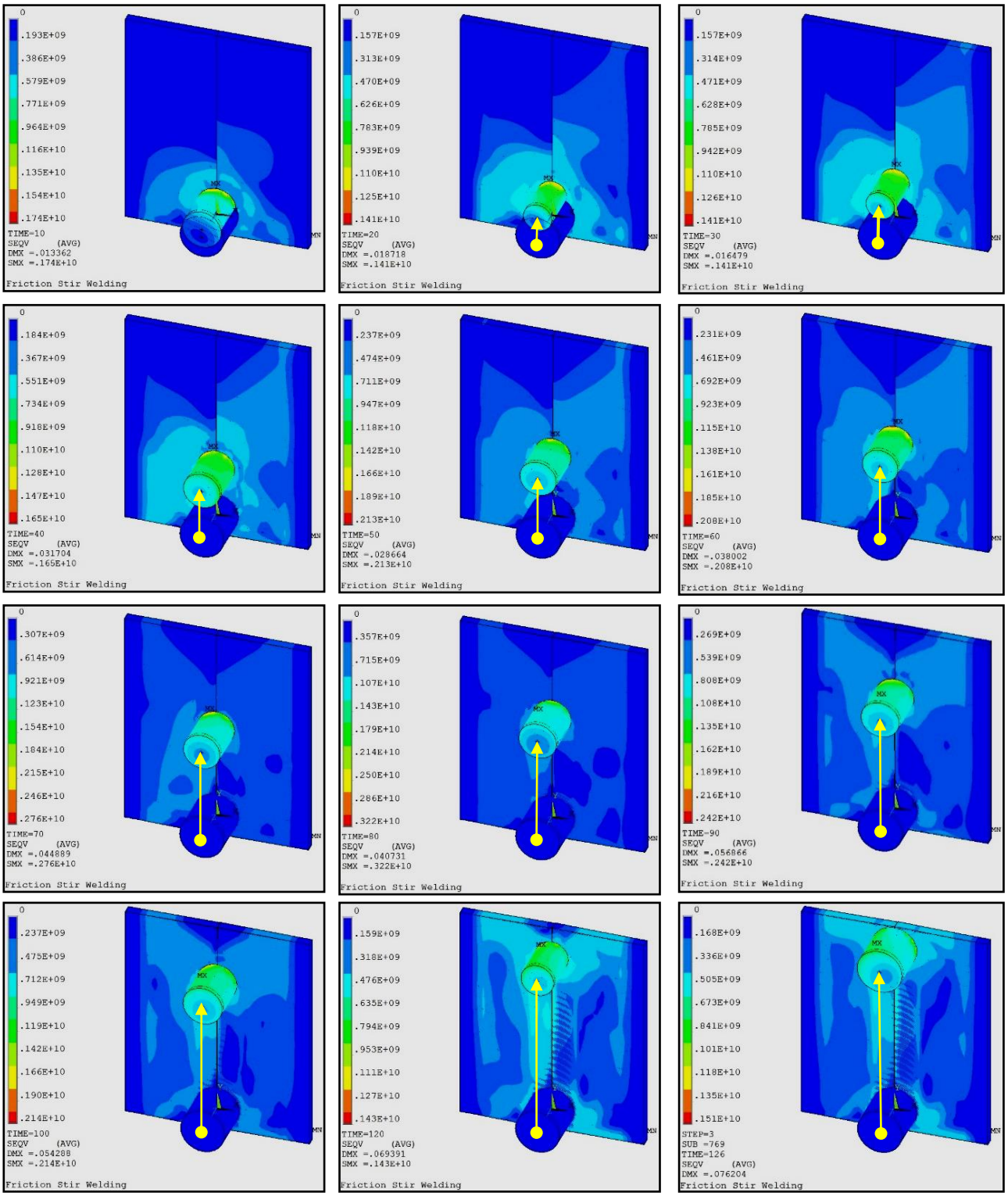

Figure 9. Von Mises stress distribution at t = 10, 20, 30, 40, 50, 60, 70, 80, 90, 100, 120 and 126.5 s for ω = 600 min^{-1} and v = 80 mm/min.

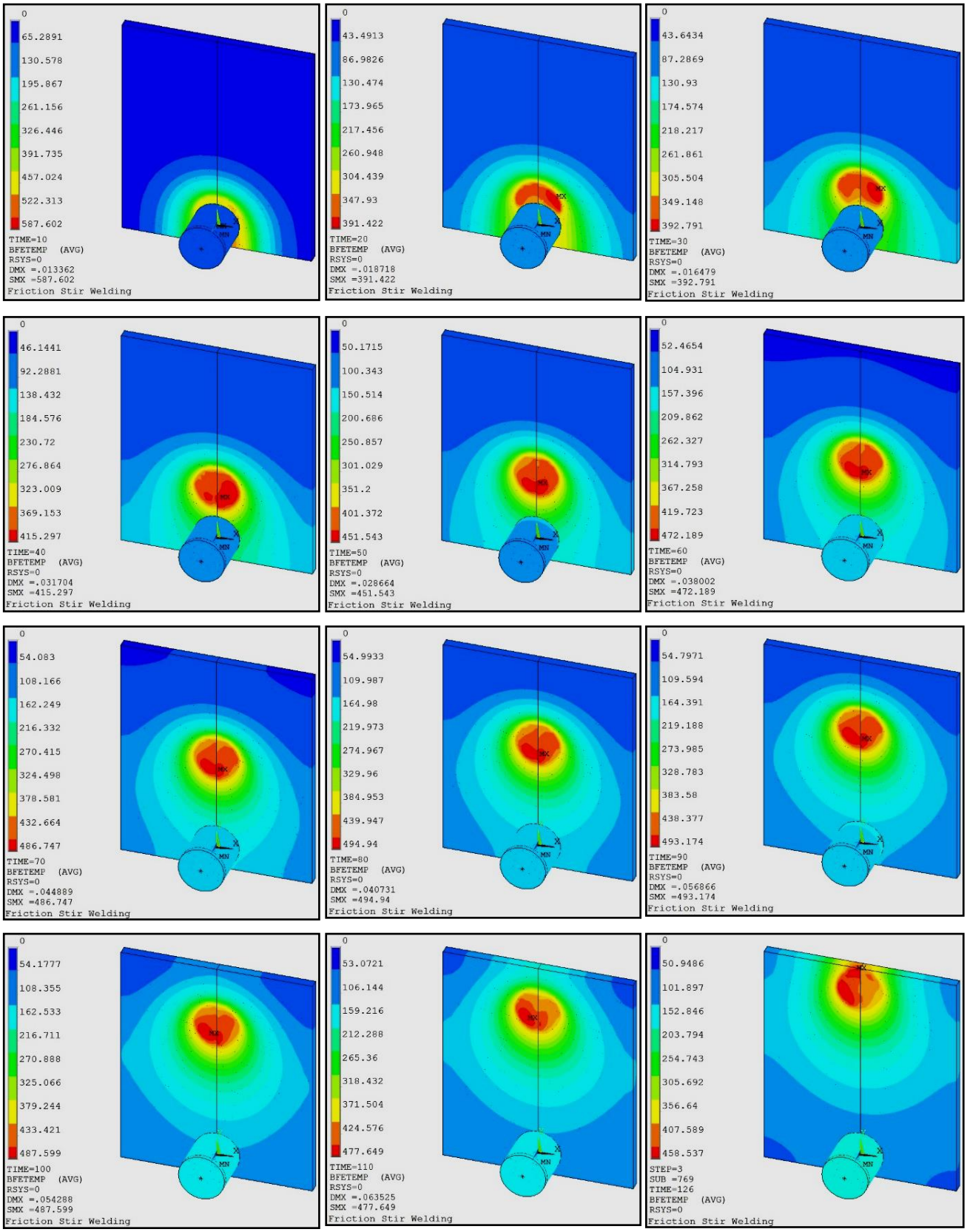

Figure 10. Temperature distributions (°C) at t = 10, 20, 30, 40, 50, 60, 70, 80, 90, 100 and 112.5 s for ω = 600 rpm and v = 80 mm/min.

Figure 11 shows Von Mises stress plots (N/m^2) at eleven characteristic time intervals: 10, 20, 30, 40, 50, 60, 70, 80, 90, 100 and 112.5 s from the start of process. At the commencement of plunging, an axial force is exerted onto the material beneath the tool pin, causing an area of high compressive stress in the workpiece with heat build-up at the pin-workpiece interface, where the material progressively softens. At 10 s the Von Mises stress in the plates under the

tool pin nearly approach 1890 MPa, caused by extremely high temperature in this area, equal to 596.77 °C, as calculated from constitutive equations. In 20 s, the distribution of Von Mises stresses in the aluminium plates decrease to 1960 MPa and migrate to a remote location from the pin-piece interface.

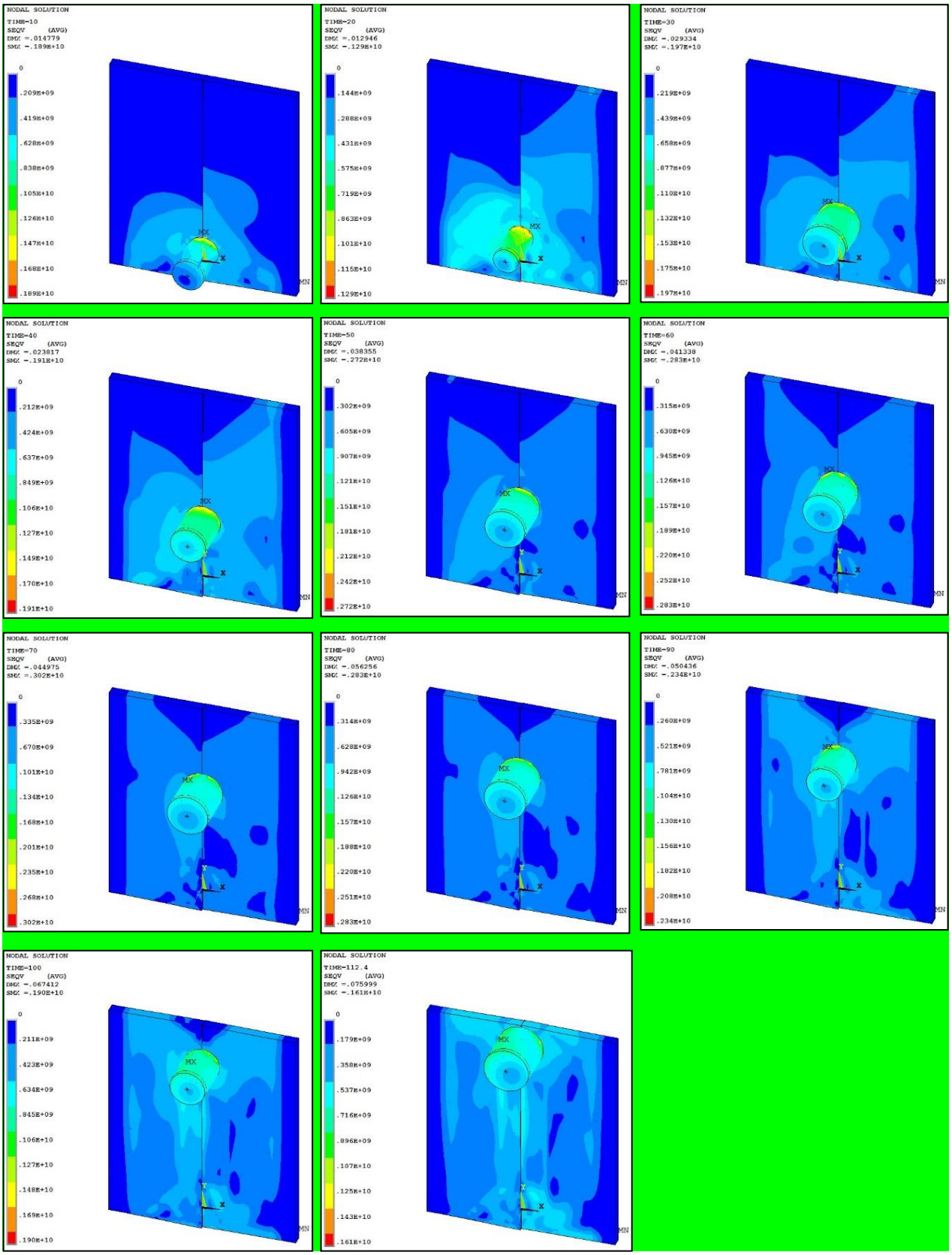

Figure 11. Von Mises stress distribution at t = 10, 20, 30, 40, 50, 60, 70, 80, 90, 100 and 112.5 s for ω = 600 rpm and v = 100 mm/min.

However, at 30, 40, 50, 60, and 70 s, in Fig. 12 we see a cylindrical layer of material surrounding the tool spindle which shows very high Von Mises stress. Constitutive equations prove the extremely high temperature in this area.

After the tool shoulder touches the workpiece at 10 s, the cylindrical high stress layer gradually disappears since the material is heated up by heat generated at the shoulder-pin interface. Most of the material under the tool is softened and in a state that it could be easily stirred. During the welding phase, from 20 to 80 s, no obvious variation of the stress field distribution around the tool is observed.

This is due to the fact that the temperature distribution around the tool after 10 s reaches a steady state as shown in Fig. 12. From the observation of the stress evolution throughout the process, it can be seen that the temperature imposes a significant effect on the stress and consequently, on the formation of the weld.

Figure 12 shows the evolution of the temperature in the length of the plate to be welded along the Y axis at t = 60 and 70 s. It is observed that the temperature regains its maximal value at the upper surface of the aluminium plate A6061-T6, equal to 526.78 and 535.12 °C, in respect, this being due to the low thickness in front of the remaining dimensions of the plate.

At 80 s weld time, the temperature decreases to 536.5 °C, but is better distributed between the front and the backside of the tool. In Fig. 12 we present a comparison of the temperature distribution on the cord line, taken at t = 10, 20, 30, 40, and 50 s for aluminium alloy Al6061-T6. The temperatures in the five instants are 596.77, 425.40, 438.53, 480.58, and 508.49 °C, and it is found that maximal temperatures are reached in the core zone of the cords, approximately 596.77 °C.

Figure 12 illustrates the temperature distribution along the junction line (cord), at t = 90 s, for aluminium alloys A6061-T6. It is observed that the passage of the FSW tool causes a rapid increase in maximum temperature, of 527.85 °C, as shown in Fig. 12.

We note in Fig. 12 at t = 100 s the temperature decreases to 515 °C. In other words, for t = 112.5 s, the temperature decreases to 494.62 °C. This decrease corresponds to the area of contact (friction) between FSW tool and the plates to be welded.

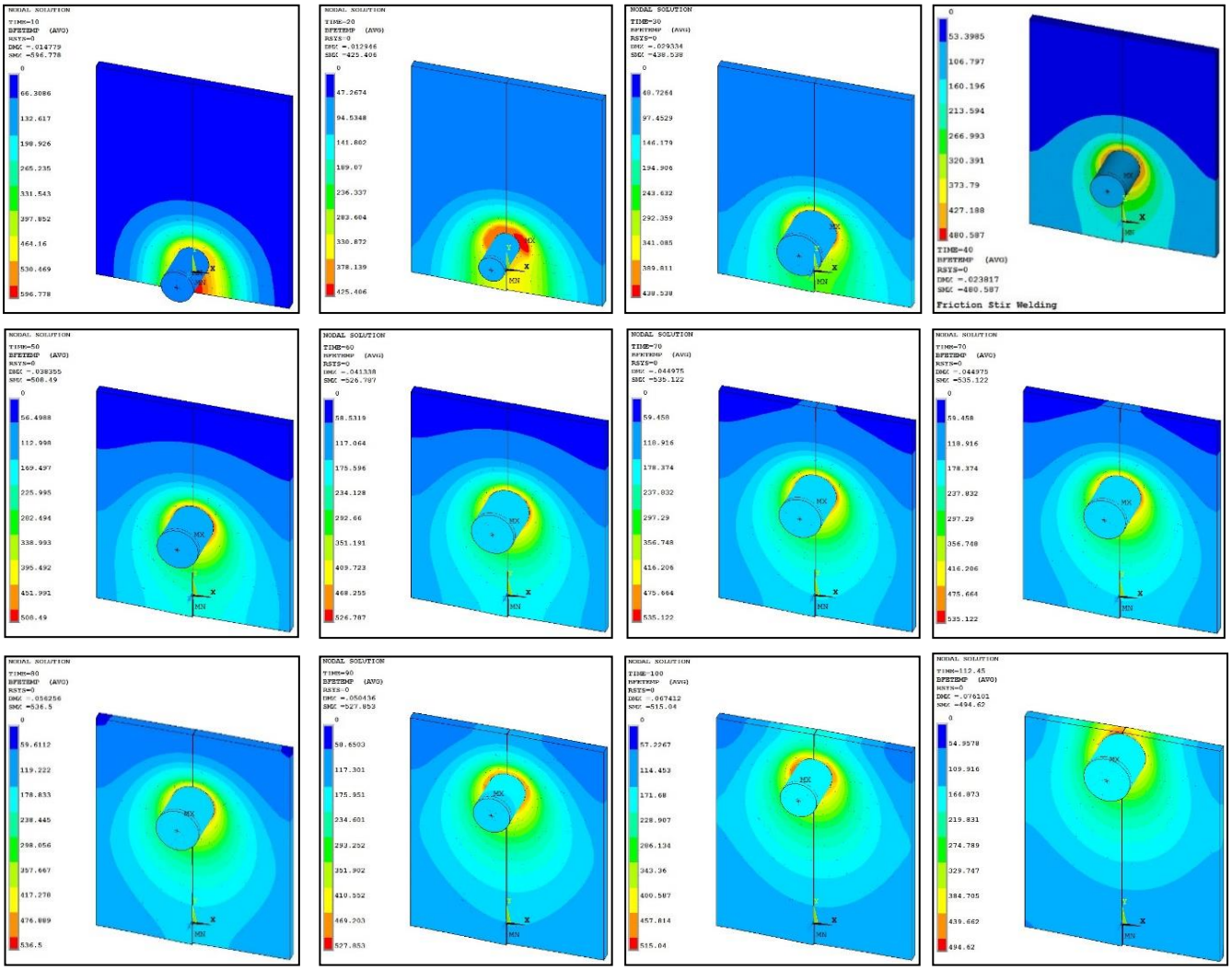

Figure 12. Temperature distributions (°C) at t = 10, 20, 30, 40, 50, 60, 70, 80, 90, 100 and 112.5 s, for ω = 600 rpm and v = 100 mm/min.

Figure 13 shows the distribution of Von Mises stress in the longitudinal line of the cord. These distributions are represented at different times for Al6061-T6 aluminium alloy. We see in this figure, at 10 s, the stress in the plates under the tool spindle has almost reached 2140 MPa, because of the extremely high temperature in this zone (618.903) °C, indicated by constituent equations.

At 10 s, the maximum Von Mises stress migrated to a location far from the pin-to-room interface. However, after welding time (20 s), there remains a cylindrical layer of material surrounding the tool spindle which exhibits a relatively low stress, by supplying to 10 s, equal to 1690 MPa as shown by the contour of Von Mises stress.

Figure 13 displays the distribution of Von Mises stress for the indicated tool at linear welding speed 140 mm/min and rotating speed 600 rpm, and for machining times 50, 60, 70, and 80 s, that are of very high contour in red. On the other hand, after the welding time 96.5 s, the Von Mises stress decreases to 1690 MPa.

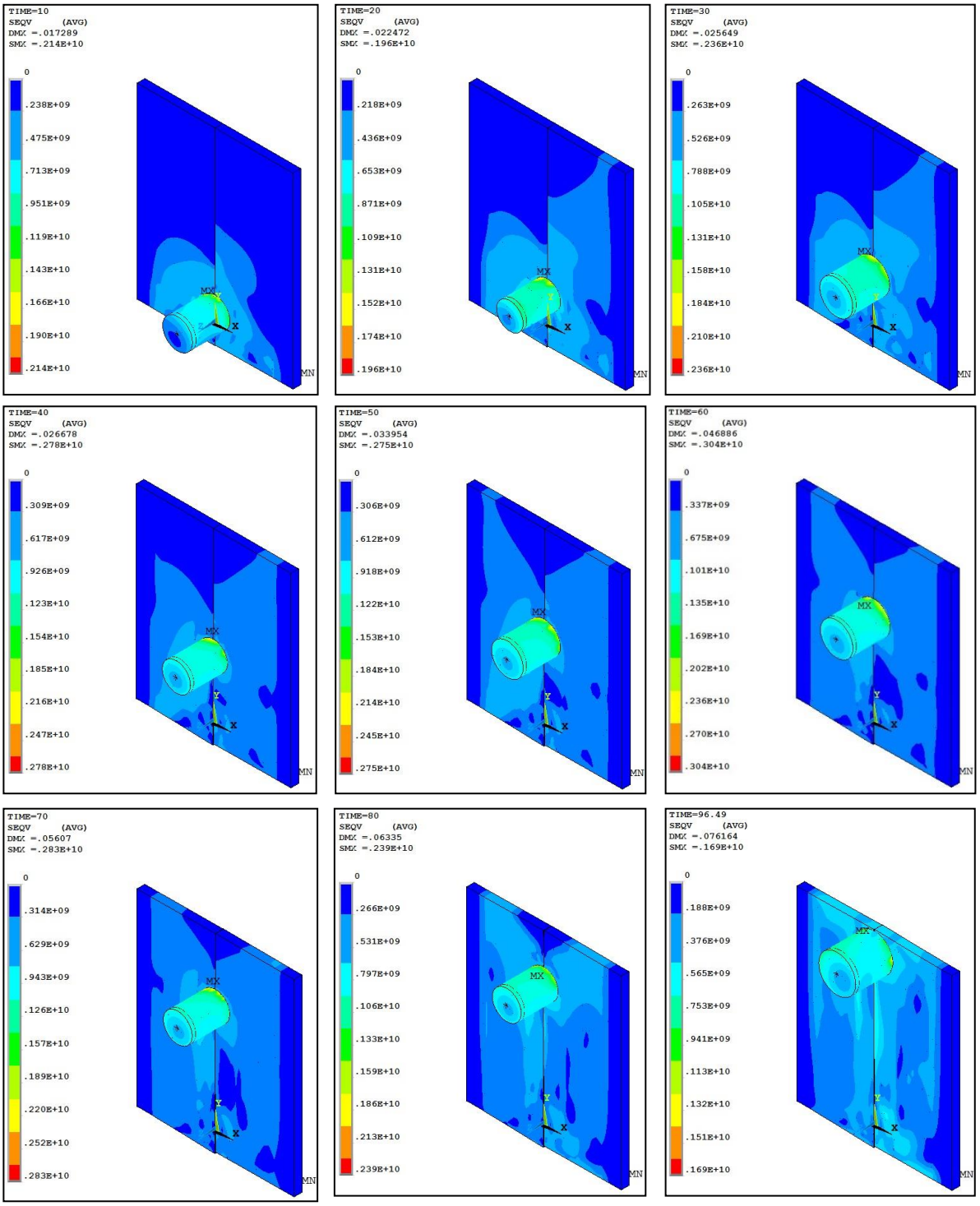

Figure 13. Von Mises stress distributions at t = 10, 20, 30, 40, 50, 60, 70, 80, 90 and 96.5 s for ω = 600 rpm and v = 140 mm/min.

Figure 14 illustrates the temperature distribution along the junction line (cord) at different welding time t = 10, 20, 30, 40, 50, 60, 70, 80, and 96.5 s for aluminium alloy A6061-T6. It is observed that the passage of the FSW tool causes rapid increase in maximal temperature. This corresponds to the area of contact (friction) between FSW tool and two plates to be welded.

In this zone the temperature gradient is zero, because the thermal flux resulting from friction is the same over the entire surface of the FSW tool shoulder. We also see that after the first three times (t = 10, 20, and 30 s) the maximal temperature values become very close. This is due to the approximation of the source to the longitudinal sample line (measurement).

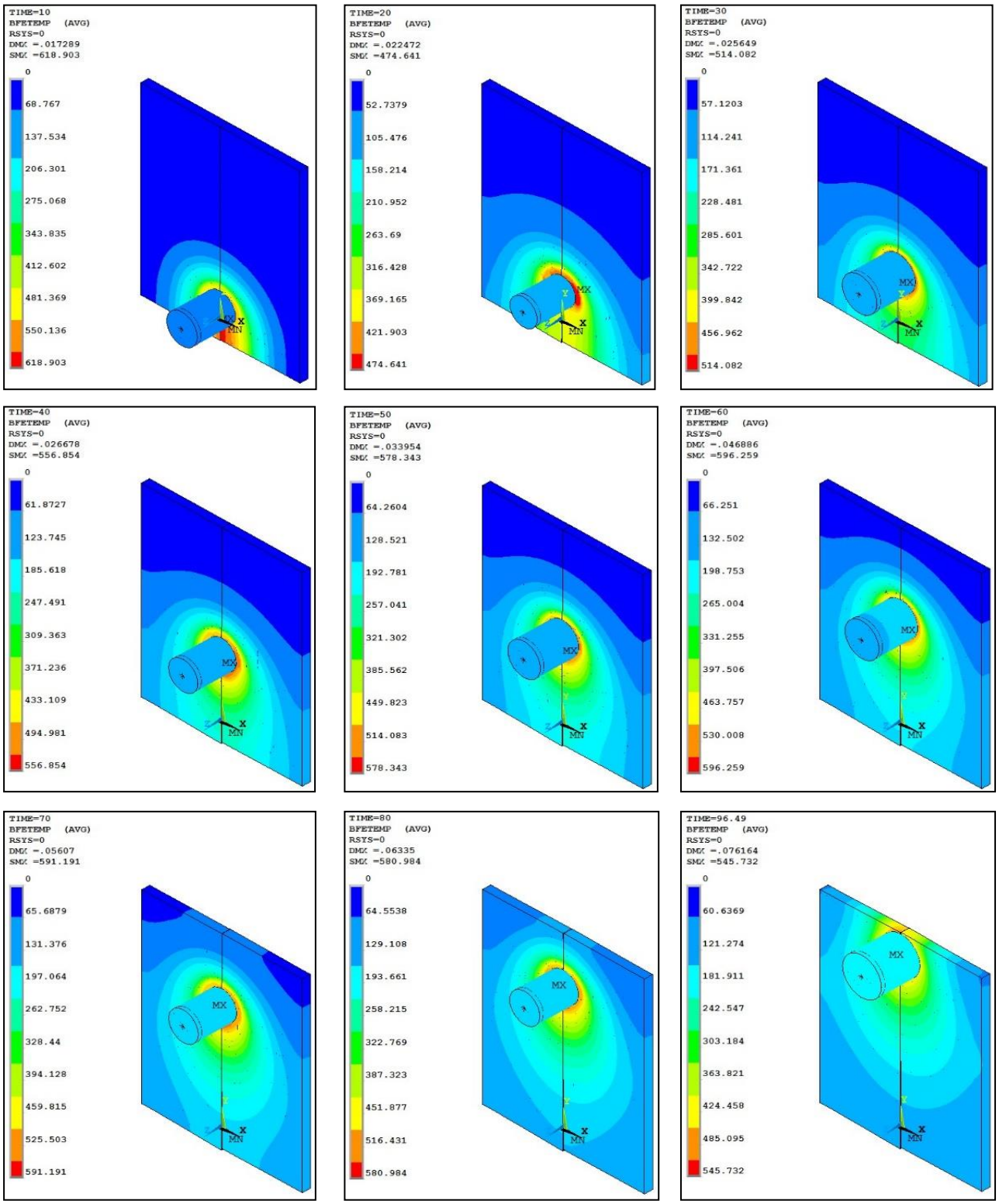

Figure 14. Temperature distributions (ºC) at t = 10, 20, 30, 40, 50, 60, 70, 80 and 96.5 s for ω = 600 rpm and v = 140 mm/min.

Plastic strain

The weld microstructure strongly depends on the thermal cycle and plastic deformation the material experiences. The ability of the model to calculate plastic strain and strain rate makes the prediction of the microstructure possible. In the present study only the plastic strain profile is discussed.

As an example, Fig. 15 illustrates equivalent plastic strain contour at 95 s along two lines, a longitudinal line (AA) between two nodes (1939, 2030), and a transverse line (BB) between two nodes (4972, 1834). We notice in Fig. 15, the tool movement on two aluminium plates with welding speed of 80 mm/min and rotation speed 600 rpm gives a stiffer welding seam. In sub-cases the maximal equivalent plastic strain of the cord equals to 0.03874. In other words, the transverse line gives maximum equivalent plastic strains equal to 0.045279, this mentioned in Fig. 15.

It is apparent that the plastic strain distribution is not symmetric about the joining line, and the advancing side has a higher average plastic strain than the retreating side. This is consistent with the findings in /27, 29/. The highest plastic region is still along the weld line with a width close to the pin diameter.

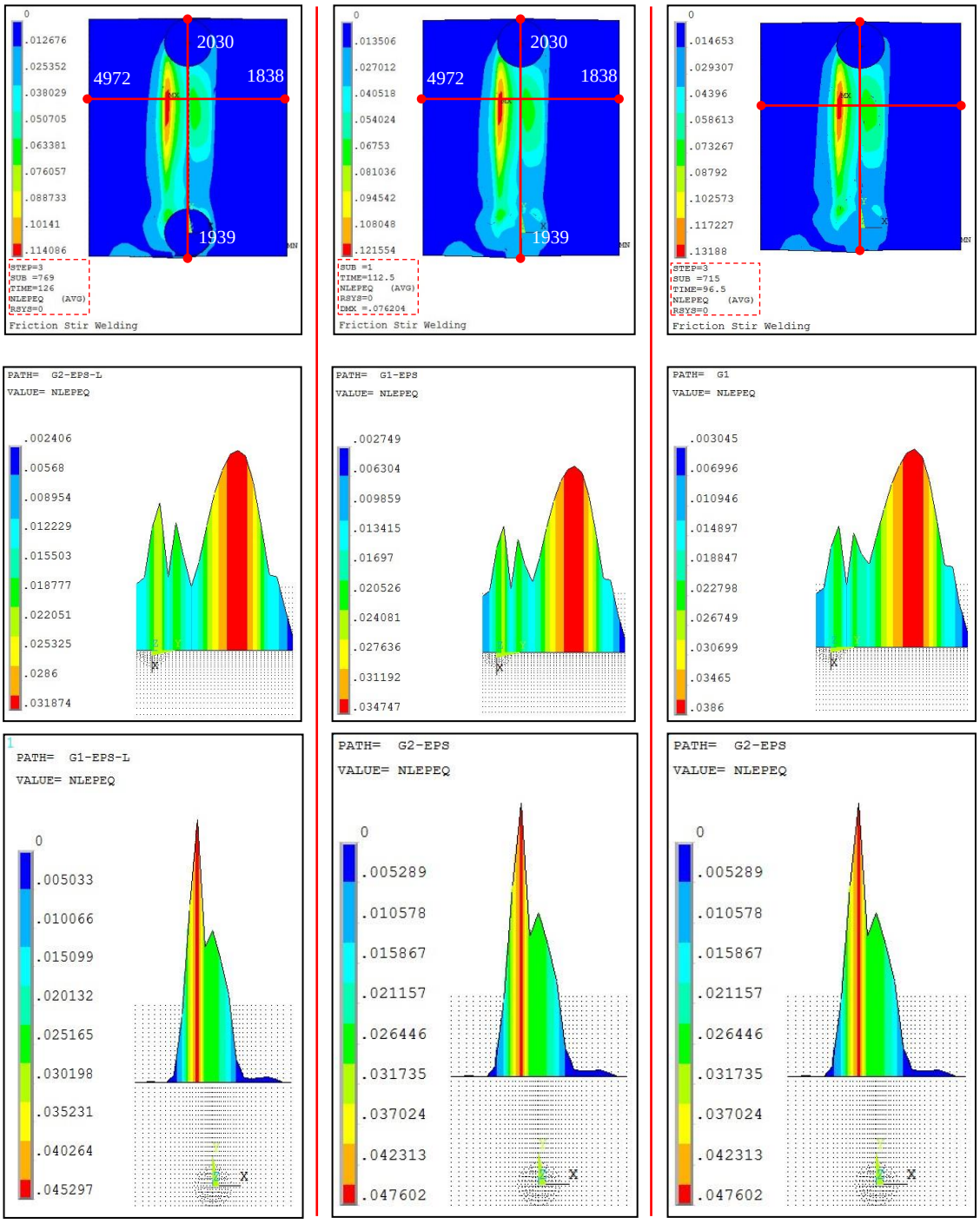

Figure 15. Simulation of equivalent plastic strain profiles for pure aluminium 6061 at different transverse speeds (constant rotating speed of 600 rpm): (a) 80 mm/min; (b) 100 mm/min; (c) 140 mm/min.

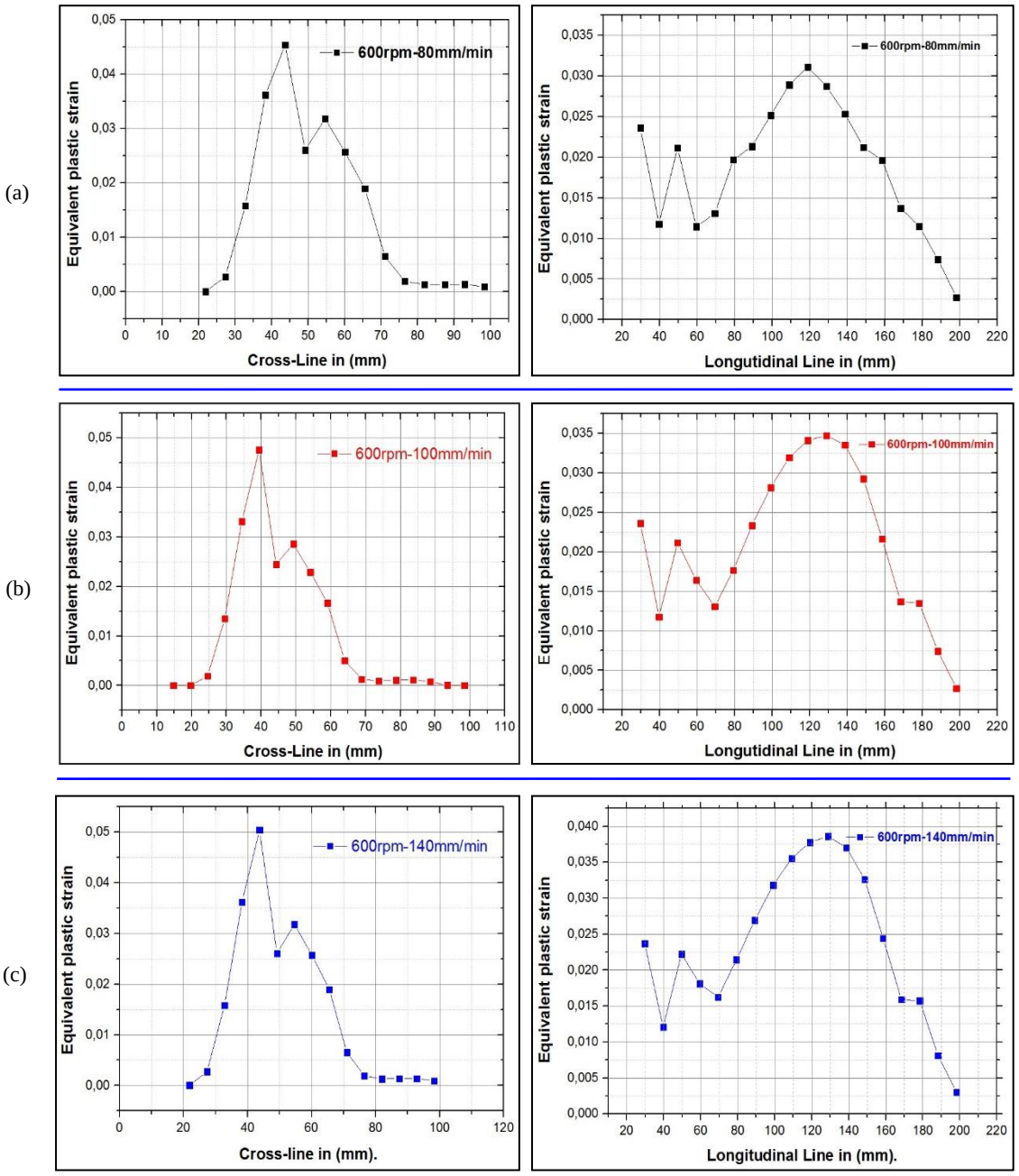

Figure 16. Equivalent plastic strain for pure aluminium 6061 at different transverse speeds (constant rotating speed 600 rpm): (a) 80 mm/min; (b) 100 mm/min; (c) 140 mm/min.

Figure. 16 shows equivalent plastic strain variation with distance for welding speeds 80, 100 and 140 mm/min, at constant rotating speed of 600 rpm. It is evident from Fig. 16 that keeping the applied force and rotating speed constant, as the welding speed increases the equivalent plastic strain increases.

CONCLUSION

The proposed finite element model of FSW has successfully simulated the plunge, dwell and traverse stages of the friction stir welding process. The development of field variables: temperature, Von Mises and residual stress, and plastic strain are quantified by the model.

Summarizing the main features of the results, the following conclusions can be drawn:

The predicted maximal temperature is higher than the melting point of the material, resulting in a lower stress field than expected around the tool during welding. Material movement is visualized by defining tracer particles at locations of interest. The numerically computed material flow patterns are in very good agreement with the general findings in experiments, and the peak temperature of the welded joint increases by increasing the welding rotation frequency for the same tool profile and welding speed. In other words, the temperature prediction results found by the FE model, never reach the fusion temperature of the material in question.

On the other hand, it is evident from the simulation that keeping the applied force and the rotational speed constant, as the welding speed increases the equivalent plastic strain

increases, and finally the residual stresses are affected by the FSW process. Moreover, the processing parameters are responsible for the types of resultant stresses, the welding temperature and mixing.

An increase in welding speed apparently leads to an increase in the residual stress. Residual stresses found by this FE model have never exceeded 54 % of the elastic limit, so we can say that the model gives good results in terms of stress.

REFERENCES

1. Savaş, A. (2016), *Investigating the influence of tool shape during FSW of aluminum alloy via CFD analysis*, J Chinese Inst. Eng. 39(2): 211-220. doi: 10.1080/02533839.2015.1091277
2. Fabregas Villegas, J., Martínez Guarin, A., Unfried-Silgado, J. (2019), *A coupled rigid-viscoplastic numerical modeling for evaluating effects of shoulder geometry on friction stir-welded aluminum alloys*, Int. J Eng. Trans. B: Appl. 32(2): 184-191. doi: 10.5829/ije.2019.32.02b.17
3. Tang, W., Guo, X., McClure, J.C., et al. (1998), *Heat input and temperature distribution in friction stir welding*, J Mater. Proc. Manuf. Sci. 7(2): 163-172. doi: 10.1106/55TF-PF2G-JBH2-1Q2B
4. Gould, J.E., Feng, Z. (1998), *Heat flow model for friction stir welding of aluminum alloys*, J Mater. Proc. Manuf. Sci. 7(2): 185-194. doi: 10.1106/648R-2CNE-2PD0-45L6
5. Chao, Y.J., Qi, X. (1998), *Thermal and thermo-mechanical modeling of friction stir welding of aluminum alloy 6061-T6*, J Mater. Process. Manuf. Sci. 7(2): 215-233. doi: 10.1106/LTKR-JFBM-RGMV-WVCF
6. Chao, Y.J., Qi, X. (1999), *Heat transfer and thermo-mechanical modeling of friction stir joining of AA6061-T6 plates*, in: Proc. 1st Intl. Symp. FSW, Thousand Oaks, CA, USA.
7. Colegrove, P., Painter, M., Graham, D., Miller, T. (2000). *3-Dimensional flow and thermal modelling of the friction stir welding process*, in: Proc. 2nd Intl. Symp. FSW, Gothenburg, Sweden.
8. Frigaard, Ø., Grong, Ø., Midling, O.T. (2001). *A process model for friction stir welding of age hardening aluminum alloys*, Metal. Mater. Trans. A 32: 1189-1200. doi:10.1007/s11661-001-0128-4
9. Midling, O.T., Rarvik, G. (1999), *Effect of tool shoulder material on heat input during friction stir welding*, in: Proc. 1st Intl. Symp. FSW, Thousand Oaks, CA, USA.
10. Russell, M.J., Sheercliff, H.R. (1999), *Analytic modeling of microstructure development in friction stir welding*, in: Proc. 1st Int. Symp. Friction Stir Welding, Thousand Oaks, CA, USA
11. Donne, C.D., Lima, E., Wegener, J., et al. (2001), *Investigations on residual stresses in friction stir welds*, in: Proc. Third Int. Symp. Friction Stir Welding, Kobe, Japan.
12. Dong, P., Lu, F., Hong, J.K., Cao, Z. (2001), *Coupled thermo-mechanical analysis of friction stir welding process using simplified models*, Sci. Technol. Weld. Joining, 6(5): 281-287. doi: 10.1179/136217101101538884
13. Chao, Y.J., Qi, X., Tang, W. (2003). *Heat transfer in friction stir welding - experimental and numerical studies*, ASME J Manuf. Sci. Eng. 125(1): 138-145. doi: 10.1115/1.1537741
14. Talwar, R., Bolser, D., Lederich, R.J, Baumann, J. (2000), *Friction stir welding of airframe structures*, in: Proc. 2nd Intl. Symp. FSW, Gothenburg, Sweden.
15. Reynolds, A.P., Lockwood, W.D., Seidel, T.U. (2000). *Processing-property correlation in friction stir welds*, Mater. Sci. Forum, 331-337: 1719-1724 doi: 10.4028/www.scientific.net/MSF.331-337.1719
16. Tekriwal, P., Mazumder, J. (1991), *Transient and residual thermal strain-stress analysis of GMAW*, J Eng. Mater. Technol. 113(3): 336-343. doi: 10.1115/1.2903415
17. Zhu, X.K., Chao, Y.J. (2002), *Effects of temperature-dependent material properties on welding simulation*, Comput. Struct. 80(11): 967-976. doi: 10.1016/S0045-7949(02)00040-8
18. Radaj, D., Heat Effects of Welding - Temperature Field, Residual Stress, Distortion, Springer-Verlag, Berlin, 1992.
19. Deng, X., Xu, S. (2001), *Solid mechanics simulation of friction stir welding process*, Trans. NAMRI-SME. 29: 631-638.
20. Chao, Y.J., Qi, X. (1998), Thermal and thermo-mechanical modeling of friction stir welding of aluminum alloy 6061-T6, J Mater. Process. Mfg. Sci. 7(2): 215-233. doi: 10.1106/LTKR-JFBM-RGMV-WVCF
21. Dong, P., Lu, F., Hong, J.K., Cao, Z. (2001). *Coupled thermo-mechanical analysis of friction stir welding process using simplified models*, Sci. Technol. Weld. Joining, 6(5): 281-287. doi: 10.1179/136217101101538884
22. Reddy, M.G., et al. (2006), *Microstructure, residual stress distribution and mechanical properties of friction-stir AA 6061 aluminium alloy weldments*, in Proc. National Sem. on NDE, Dec. 7-9, 2006, Hyderabad, India.
23. Brahami, A., Bouchouicha, B., Zemri, M., Fajoui, J. (2018), *Fatigue crack growth rate, microstructure and mechanical properties of diverse range of aluminum alloy: a comparison*, Mech. & Mechanical Eng. 22(1): 329-339.
24. Moaveni, S., Finite Element Analysis Theory and Application with ANSYS, 3rd Ed., Prentice-Hall, Inc., NJ, USA, 2007.
25. Bastier, A., Modélisation du soudage d'alliages d'aluminium par friction et malaxage. Ph.D. thesis, École Polytechnique, France, 2006. (Français)
26. Chen, C., Kovacevic, R. (2004). *Thermomechanical modelling and force analysis of friction stir welding by the finite element method*, Proc. Instn. Mech. Engrs. Part C: J Mech. Eng. Sci. 218(5): 509-519. doi: 10.1243/095440604323052292
27. Singarapu, U., Adepu, K. Arumalle, S.R. (2015), *Influence of tool material and rotational speed on mechanical properties of friction stir welded AZ31B magnesium alloy*, J Magnesium and Alloys, 3(4): 335-344. doi: 10.1016/j.jma.2015.10.001
28. Heurtier, P., Desrayaud, C., Montheillet, F. (2002), *A thermo-mechanical analysis of the friction stir welding process*, Mater. Sci. Forum, 396-402(3): 1537-1542. doi: 10.4028/www.scientific.net/MSF.396-402.1537
29. Buffa, G., Hua, J., Shivpuri, R., Fratini, L. (2006), *A continuum based fem model for friction stir welding-model development*, Mater. Sci. Eng. 419(1-2): 389-396. doi: 10.1016/j.msea.2005.09.040